arXiv:2108.13616v2 [math.NA] 1 Sep 2021

An Efficient Finite Element Iterative Method for Solving a Nonuniform Size Modified Poisson-Boltzmann Ion Channel Model

Dexuan Xie*

Abstract

In this paper, a nonuniform size modified Poisson-Boltzmann ion channel (nuSMPBIC) model is presented as a nonlinear system of an electrostatic potential and multiple ionic concentrations. It mixes nonlinear algebraic equations with a Poisson boundary value problem involving Dirichlet-Neumann mixed boundary value conditions and a membrane surface charge density to reflect the effects of ion sizes and membrane charges on electrostatics and ionic concentrations. To overcome the difficulties of strong singularities and exponential nonlinearities, it is split into three submodels with a solution of Model 1 collecting all the singular points and Models 2 and 3 much easier to solve numerically than the original nuSMPBIC model. A damped two-block iterative method is then presented to solve Model 3, along with a novel modified Newton iterative scheme for solving each related nonlinear algebraic system. To this end, an effective nuSMPBIC finite element solver is derived and then implemented as a program package that works for an ion channel protein with a three-dimensional molecular structure and a mixture solution of multiple ionic species. Numerical results for a voltage-dependent anion channel (VDAC) in a mixture of four ionic species demonstrate a fast convergence rate of the damped two-block iterative method, the high performance of the software package, and the importance of considering nonuniform ion sizes. Moreover, the nuSMPBIC model is validated by the anion selectivity property of VDAC.

1 Introduction

The Poisson-Boltzmann equation (PBE) is one widely-used dielectric continuum model for the calculation of electrostatic solvation free energies [5, 6, 7, 14, 16, 18]. But it cannot distinguish the two ions with the same charge, such as cations Na^+ and K^+, since it treats ions as volume-less points. Thus, it may work poorly in the applications in which ion sizes have impact on electrostatics and ionic concentrations, especially in the simulation of ion transport across a membrane via an ion channel pore. Thus, it is important to develop size modified PBE (SMPBE) models.

*Department of Mathematical Sciences, University of Wisconsin-Milwaukee, Milwaukee, WI, 53201-0413, USA

The first SMPBE model was reported in 1997 for an asymmetric electrolyte consisting of two ionic species under the assumption that all the ions have the same size [3]. Since then, several SMPBE models had been developed for the case of a protein in an ionic solvent. For example, one SMPBE model for a protein in a solution of multiple ionic species was reported in [8]. Since it treats all the ions and water molecules as cubes, this model has a void problem (i.e., there exist cavities among ions and water molecules) in the nonuniform ion size case, breaking down the required size constraint conditions. This drawback was fixed by introducing a concentration of voids model in [11, Eq. (10)], from which another SMPBE model could be constructed. But how to estimate a concentration of voids is still a puzzle since the voids can have different shapes and different volumes. Besides, these two SMPBE models suffer a redundancy problem because they use a concentration of water molecules to describe the water solution that has been treated as a continuum dielectric in their constructions. To fix these drawbacks, several improved SMPBE models were reported in [9, 10, 19, 24], along with their effective finite element solvers and a web server [23]. Most recently, a size modified Poisson-Boltzmann ion channel (SMPBIC) model and its effective finite element solver were reported in [20]. While it can partially reflect the effect of distinct ion sizes due to setting each ion to have an average of ion sizes, this SMPBIC model still cannot distinguish the two ions with the same charge. As the continuation of this previous work, the purpose of this work is to develop a nonuniform SMPBIC (nuSMPBIC) model and its finite element solver for an ion channel protein in a mixture of multiple ionic species.

However, the nuSMPBIC model is much more difficult to solve numerically than the SMPBIC model since it is a nonlinear system mixing n nonlinear algebraic equations with one Poisson dielectric interface boundary value problem and involves two physical domains — a simulation box domain for potential functions and a solvent domain for ionic concentration functions, not to mention its stronger singularities and stronger nonlinearities than the case of a protein surrounded by an ionic solvent. Here n is the number of ionic species; the algebraic equations describe ion size constraint conditions; and the Poisson problem involves Dirichlet-Neumann mixed boundary value conditions and a membrane surface charge density to reflect membrane charge effects. A nuSMPBIC solution gives n ionic concentration functions c_i and an electrostatic potential function u. Since c_i and u are defined in two different domains, they belong to two different finite element function spaces, producing a two-domain issue that we must deal with during the development of a nuSMPBIC finite element solver. Currently, this issue was simply treated by letting c_i belong to the function space of u through setting c_i to be zero at the mesh points outside a solvent region [19]. But this simple treatment may cause a large error disturbance since it produces an artificial boundary layer around the solvent region, where c_i may have large values due to strong atomic charges on a part of solvent domain boundary — a part of an ion charge molecular surface including the mostly charged charge ion channel pore surface. To avoid such a boundary layer error, in this work, we treat this two physical domain issue directly through constructing two finite element function spaces: one for concentration functions and the other for potential functions. We then construct two communication operators to directly carry out operations involving ionic concentrations and potential functions.

Following what was done in [20], we will overcome the difficulties of solution singularities through splitting the nuSMPBIC model into three submodels, called Models 1, 2 and 3. While Models 1 and 2 are the same as those reported in [20], Model 3 is a nonlinear system

mixing the n nonlinear algebraic equations with an interface boundary value problem. A solution of Model 1 gives a potential component, G, induced by the atomic charges of an ion channel protein, in an algebraic expression that collects all the solution singularity points while a solution of Model 2 gives a potential component, Ψ, induced by membrane charges and Dirichlet boundary and interfaces values. Solving Model 3 gives n ionic concentration functions c_i and a potential component function, $\tilde{\Phi}$, induced by ionic charges from the solvent region D_s. Model 2 has been solved efficiently in [20]. Hence, we only need to develop a nonlinear iterative scheme for solving Model 3 in this work.

The classical nonlinear successive over-relaxation (SOR) iterative technique [15] is often used to develop iterative schemes for solving a system of nonlinear equations because it can separate each equation from the others so that each equation can be solved one-by-one to achieve the goal of reducing computational complexity and computer memory requirement. It was applied to the construction of a nonlinear SOR-Newton iterative scheme for solving a nonuniform SMPBE model in the case of a protein surrounded by an ionic solvent [19]. Thus, we started with an adoption of this scheme as a Model 3 solver. Unfortunately, this adapted SOR-Newton scheme was found numerically not to work well due to a slow rate of convergence because an ion channel protein has a much more complicated geometry and much stronger atomic charges than the protein case considered in [19]. Hence, developing efficient iterative schemes for solving Model 3 becomes one key step in the construction of an effective nuSMPBIC finite element solver.

During the search for an efficient Model 3 solver, we discovered that under a linear finite element framework, all the nonlinear algebraic equations of Model 3 can be split from a large set of nN_h nonlinear algebraic equations into N_h small sets with each set containing only n nonlinear algebraic equations. Here N_h is the number of mesh points of a solvent region mesh. Since n is typically very small (such as 2, 3, or 4) in practice, each small set can be quickly solved as a small nonlinear algebraic system. This discovery motivated us to divide the equations of Model 3 into two blocks — Block 1 consists of all the nonlinear algebraic equations and Block 2 contains the linear boundary problem only. We then construct a novel modified Newton iterative scheme to solve the nonlinear algebraic equations of Block 1 quickly, resulting in an efficient damped two-block iterative method for solving Model 3. In addition, we construct a linearized SMPBIC model and use its finite element solution as a good initial iterate of the damped two-block iterative method. Consequently, the construction of an efficient nuSMPBIC finite element solver is completed.

Finally, we implemented this new nuSMPBIC finite element solver in Python and Fortran as a software package based on the state-of-the-art finite element library from the FEniCS project [13] and the SMPBIC program package [20]. To demonstrate the performance of the new nuSMPBIC software package, we did numerical tests using a crystallographic three-dimensional molecular structure of a murine voltage-dependent anion channel 1 (mVDAC1) [17] in a mixture solution of four ionic species. Note that this mVDAC1 protein (PBD ID: 3EMN) is known to be in the open state conformation with an anion selectivity property. Hence, it can serve as a good test case for assessing our nuSMPBIC model. Numerical results demonstrate a fast convergence rate of our damped two-block iterative method, the high performance of our nuSMPBIC software package, and the importance of considering nonuniform ion sizes. They also show that the membrane surface charges have impact on the electrostatic potential and ionic concentrations. Moreover, our SMPBIC model was validated

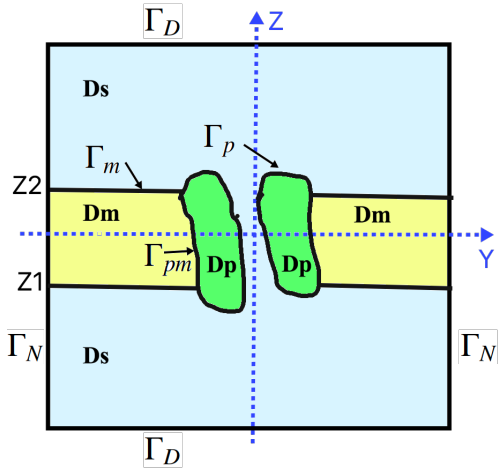


Figure 1: An illustration of a box domain partition given in (2) and (3).

by the mVDAC1 anion selectivity property.

The remaining part of the paper is arranged as follows. In Section 2, we present the nuSMPBIC model. In Section 3, we split the nuSMPBIC model into three submodels. In Section 4, we present the damped two-block iterative method. In Section 5, we present the Newton iterative scheme for solving each nonlinear algebraic system arisen from the damped two-block iterative method. In Section 6, we construct a good initial iterate for the damped two-block iterative method. In Section 7, we report the nuSMPBE program package and numerical test results. Finally, conclusions are made in Section 8.

2 A nonuniform size modified Poisson-Boltzmann ion channel model

We define a simulation box domain, Ω, by

$$\Omega = \{(x, y, z) \mid L_{x1} < x < L_{x2},\ L_{y1} < y < L_{y2},\ L_{z1} < z < L_{z2}\ \}, \tag{1}$$

and split it into three open subdomains, D_p, D_m, and D_s as follows:

$$\Omega = D_p \cup D_m \cup D_s \cup \Gamma_p \cup \Gamma_m \cup \Gamma_{pm}, \tag{2}$$

where $L_{x1}, L_{x2}, L_{y1}, L_{y2}, L_{z1}$, and L_{z2} are real numbers; D_p is a protein region containing an ion channel protein molecule with n_p atoms; D_m is a membrane region; D_s is a solvent region containing n ionic species; Γ_p denotes an interface between D_p and D_s; Γ_m an interface between D_m and D_s; and Γ_{pm} an interface between D_p and D_m. We also split the boundary $\partial\Omega$ of Ω by

$$\partial\Omega = \Gamma_D \cup \Gamma_N, \tag{3}$$

where Γ_D consists of the bottom and top surfaces of Ω and Γ_N consists of the four side surfaces of Ω. We further set the normal direction of the membrane surface in the z-axis direction so that the membrane location can be determined by two numbers $Z1$ and $Z2$. An illustration of this setting and partitions (2) and (3) is given in Figure 1.

Let c_i denote a concentration function of the i-th species in moles per liter (mol/L) and u be a dimensionless electrostatic potential function of an electric field induced by

atomic charges, ionic charges, and membrane charges. When a three-dimensional molecular structure of an ion channel protein and a mixture solution of n ionic species are given, an atomic charge density function, ρ_p, and an ionic charge density function, ρ_s, can be estimated by

$$\rho_p = e_c \sum_{j=1}^{n_p} z_j \delta_{\mathbf{r}_j} \quad \text{in } D_p, \qquad \rho_s(\mathbf{r}) = e_c \sum_{i=1}^{n} Z_i c_i(\mathbf{r}) \quad \text{in } D_s,$$

where e_c is the elementary charge, z_j and $\mathbf{r}_j$ denote the atomic charge number and position vector of atom j, respectively, Z_i is the charge number of ionic species i, and $\delta_{\mathbf{r}_j}$ is the Dirac delta distribution at $\mathbf{r}_j$. In addition, a membrane surface charge density σ is given in $\mu\text{C/cm}^2$ to account for membrane charge effects. Based on the implicit solvent approach, the three regions D_p, D_m, and D_s are treated as dielectric media with permittivity constants ϵ_p, ϵ_m, and ϵ_s, respectively. We then construct a Poisson dielectric boundary value problem for estimating u as follows:

$$\begin{cases} -\epsilon_p \Delta u(\mathbf{r}) = \alpha \sum_{j=1}^{n_p} z_j \delta_{\mathbf{r}_j}, & \mathbf{r} \in D_p, \\ -\epsilon_m \Delta u(\mathbf{r}) = 0, & \mathbf{r} \in D_m, \\ -\epsilon_s \Delta u(\mathbf{r}) = \beta \sum_{i=1}^{n} Z_i c_i(\mathbf{r}), & \mathbf{r} \in D_s, \\ u(\mathbf{s}^-) = u(\mathbf{s}^+), \quad \epsilon_p \frac{\partial u(\mathbf{s}^-)}{\partial \mathbf{n}_p(\mathbf{s})} = \epsilon_s \frac{\partial u(\mathbf{s}^+)}{\partial \mathbf{n}_p(\mathbf{s})}, & \mathbf{s} \in \Gamma_p, \\ u(\mathbf{s}^-) = u(\mathbf{s}^+), \quad \epsilon_m \frac{\partial u(\mathbf{s}^-)}{\partial \mathbf{n}_m(\mathbf{s})} = \epsilon_s \frac{\partial u(\mathbf{s}^+)}{\partial \mathbf{n}_m(\mathbf{s})} + \tau\sigma, & \mathbf{s} \in \Gamma_m, \\ u(\mathbf{s}^-) = u(\mathbf{s}^+), \quad \epsilon_p \frac{\partial u(\mathbf{s}^-)}{\partial \mathbf{n}_p(\mathbf{s})} = \epsilon_m \frac{\partial u(\mathbf{s}^+)}{\partial \mathbf{n}_p(\mathbf{s})}, & \mathbf{s} \in \Gamma_{pm}, \\ u(\mathbf{s}) = g(\mathbf{s}), & \mathbf{s} \in \Gamma_D, \\ \frac{\partial u(\mathbf{s})}{\partial \mathbf{n}_b(s)} = 0, & s \in \Gamma_N, \end{cases} \tag{4}$$

where $\mathbf{n}_s$, $\mathbf{n}_p$, $\mathbf{n}_m$, and $\mathbf{n}_b$ denote the unit outward normal directions of D_s, D_p, D_m, and Ω, respectively; $\frac{\partial u(\mathbf{s})}{\partial \mathbf{n}(\mathbf{s})}$ denotes the directional derivative of u along a unit outside normal direction $\mathbf{n}$ (say, $\mathbf{n} = \mathbf{n}_p$); $u(\mathbf{s}^\pm) = \lim_{t \to 0^+} u(\mathbf{s} \pm t\mathbf{n}(\mathbf{s}))$, which are the two sided limits along a direction $\mathbf{n}$ of a region (say a protein region, D_p) from the inside and outside the region; α, β and τ are three physical constants; and g is a boundary value function. Here the SI unit system has been used and the constants α, β and τ are defined by

$$\alpha = \frac{10^{10} e_c^2}{\epsilon_0 k_B T}, \quad \beta = \frac{N_A e_c^2}{10^{17} \epsilon_0 k_B T}, \quad \tau = \frac{10^{-12} e_c}{\epsilon_0 k_B T}, \tag{5}$$

where ϵ_0 is the permittivity of the vacuum, k_B is the Boltzmann constant, T is the absolute temperature, and N_A is the Avogadro number, which estimates the number of ions per mole.

From the Poisson problem (4) it can be seen that different selections of ionic concentrations c_i may lead to different electrostatic potentials u. To find an optimal selection, we define an electrostatic free energy functional, $F(c; u)$, by

$$F(c; u) = F_{es}(c; u) + F_{id}(c) + F_{ex}(c) \qquad \text{with} \quad c = (c_1, c_2, \ldots, c_n), \tag{6}$$

where F_{es}, F_{id}, and F_{ex} denote the electrostatic, ideal gas, and excess energies, respectively,

in the expressions

$$\begin{aligned} F_{es}(c;u) &= \frac{k_BT}{2}\gamma\sum_{i=1}^{n} Z_i\int_{D_s} uc_i d\mathbf{r}, \quad F_{id}(c) = k_BT\gamma\sum_{i=1}^{n}\int_{D_s} c_i\left(\ln\frac{c_i}{c_i^b}-1\right)d\mathbf{r}, \\ F_{ex}(c) &= \frac{k_BT}{v_0}\int_{D_s}\left[1-\gamma\sum_{i=1}^{n} v_ic_i(\mathbf{r})\right]\left[\ln\left(1-\gamma\sum_{i=1}^{n} v_ic_i(\mathbf{r})\right)-1\right]d\mathbf{r}. \end{aligned}$$

Here, v_i a volume of each ion of species i in cubic angstroms (Å^3), $\gamma = 10^{-27}N_A$, c_i^b is a bulk concentration, and v_0 a size scaling parameter (e.g., $v_0 = \min_i v_i$). Note that the sum $\gamma\sum_{i=1}^{n} v_ic_i(\mathbf{r})$ gives the ionic volume portion out of the solvent region. Hence, the difference $1-\gamma\sum_{i=1}^{n} v_ic_i(\mathbf{r})$ is the portion of water solution volume, which should be positive, ensuring the definition of excess energy F_{ex}. These energy terms have been measured in energy units Joules.

The constant γ is a unit converter from mol/L to Å^3. In fact, under the SI unit system, a concentration is measured in the number of ions per Å^3. But in practice, it is usually measured in mol/L as done in this paper. Hence, γ is needed to convert from mol/L to Å^3 as shown below:

$$1 \text{ mol } /\text{L} = 10^3 N_A/m^3 = 10^{-27}N_A/\text{Å}^3 = \gamma/\text{Å}^3,$$

where we have used the unit converters: 1 mol = 1 N_A, 1 L = $m^3/10^3$, and 1 m = 10^{10} Å. For $\text{N}_A = 6.02214129\times10^{23}$, γ can be estimated as $\gamma \approx 6.022\times10^{-4}$.

The free energy functional F of (6) is a significant improvement of the conventional free energies (e.g., [8, eq. (1.4) or (3.4)], and [2, eq. (4)] or [22, eq. (36)]) since it discards the thermal de Broglie wavelengths, chemical potentials, a concentration of water molecules, and terms $\ln(v_ic_i)$.

The first Fréchet derivative F' of F can be found in the expression

$$F'(c;u)w = k_BT\gamma\sum_{i=1}^{n}\int_{D_s}\left[Z_iu+\ln\left(\frac{c_i}{c_i^b}\right)-\frac{v_i}{v_0}\ln\left(1-\gamma\sum_{j=1}^{n} v_jc_j\right)\right]w_i(\mathbf{r})d\mathbf{r},$$

where $F'(c;u)$ is a linear operator and w denotes a test function vector with $w = (w_1, w_2, \ldots, w_n)$. From the above expression we can obtain the variation $\frac{\partial F(c;u)}{\partial c_i}$ of F with respect to c_i as follows:

$$\frac{\partial F(c;u)}{\partial c_i} = k_BT\gamma\left[Z_iu+\ln\left(\frac{c_i}{c_i^b}\right)-\frac{v_i}{v_0}\ln\left(1-\gamma\sum_{j=1}^{n} v_jc_j\right)\right], \quad i=1,2,\ldots,n.$$

Setting $\frac{\partial F(c;u)}{\partial c_i} = 0$ gives the equation $Z_iu+\ln\left(\frac{c_i}{c_i^b}\right)-\frac{v_i}{v_0}\ln\left(1-\gamma\sum_{j=1}^{n} v_jc_j\right)=0$, which can be reformulated as

$$c_i(\mathbf{r}) - c_i^b\left[1-\gamma\sum_{j=1}^{n} v_jc_j(\mathbf{r})\right]^{\frac{v_i}{v_0}} e^{-Z_iu(\mathbf{r})} = 0, \quad i=1,2,\ldots,n. \tag{7}$$

Obviously, the above nonlinear algebraic equations give the necessary conditions that an optimal c must satisfy. They also can be regarded as the ion size constraint conditions during a search process for an optimal u. Because the nonlinear equations (7) and the Poisson problem (4) are dependent each other, they must be combined together as a nonlinear system in terms of c and u. A solution of this system gives an optimal c and an optimal u in the sense of minimizing the electrostatic free energy (6). This nonlinear system defines a nonuniform size modified Poisson-Boltzmann ion channel (nuSMPBIC) mode. For clarity, we restate it as follows:

$$\begin{cases} c_i(\mathbf{r}) - c_i^b \left[1 - \gamma \sum_{j=1}^{n} v_j c_j(\mathbf{r})\right]^{\frac{v_i}{v_0}} e^{-Z_i u(\mathbf{r})} = 0, & \mathbf{r} \in D_s, \quad i = 1, 2, \ldots, n, \\ -\epsilon_p \Delta u(\mathbf{r}) = \alpha \sum_{j=1}^{n_p} z_j \delta_{\mathbf{r}_j}, & \mathbf{r} \in D_p, \\ -\epsilon_m \Delta u(\mathbf{r}) = 0, & \mathbf{r} \in D_m, \\ \epsilon_s \Delta u(\mathbf{r}) - \beta \sum_{i=1}^{n} Z_i c_i(\mathbf{r}) = 0, & \mathbf{r} \in D_s, \\ u(\mathbf{s}^-) = u(\mathbf{s}^+), \quad \epsilon_p \frac{\partial u(\mathbf{s}^-)}{\partial \mathbf{n}_p(\mathbf{s})} = \epsilon_s \frac{\partial u(\mathbf{s}^+)}{\partial \mathbf{n}_p(\mathbf{s})}, & \mathbf{s} \in \Gamma_p, \\ u(\mathbf{s}^-) = u(\mathbf{s}^+), \quad \epsilon_m \frac{\partial u(\mathbf{s}^-)}{\partial \mathbf{n}_m(\mathbf{s})} = \epsilon_s \frac{\partial u(\mathbf{s}^+)}{\partial \mathbf{n}_m(\mathbf{s})} + \tau\sigma, & \mathbf{s} \in \Gamma_m, \\ u(\mathbf{s}^-) = u(\mathbf{s}^+), \quad \epsilon_p \frac{\partial u(\mathbf{s}^-)}{\partial \mathbf{n}_p(\mathbf{s})} = \epsilon_m \frac{\partial u(\mathbf{s}^+)}{\partial \mathbf{n}_p(\mathbf{s})}, & \mathbf{s} \in \Gamma_{pm}, \\ u(\mathbf{s}) = g(\mathbf{s}), & \mathbf{s} \in \Gamma_D, \\ \frac{\partial u(\mathbf{s})}{\partial \mathbf{n}_b(s)} = 0, & s \in \Gamma_N. \end{cases} \tag{8}$$

In physics, the Neumann boundary condition on the four side surface Γ_N reflects the fact that none of the charges enter the box domain Ω from Γ_N. To mimic a voltage across the membrane, we set the boundary function g as a piecewise function:

$$g(\mathbf{s}) = \begin{cases} u_b & \text{at } z = L_{z1} \text{ (bottom surface)}, \\ u_t & \text{at } z = L_{z2} \text{ (top surface)}, \end{cases} \tag{9}$$

where u_b and u_t denote two electrostatic potential values.

The nuSMPBIC model involves Dirac delta distributions, two physical domains (the solvent domain D_s and the box domain Ω), complicated interface conditions, mixed boundary value conditions (i.e., a Dirichlet boundary condition on Γ_D and a Neumann boundary condition on Γ_N), and the membrane surface charge density σ. The Dirac delta distributions cause the potential function u strongly singular while the nonlinear algebraic equations cause the ionic concentrations c_i exponentially nonlinear. Hence, the nuSMPBIC model (8) is very difficult to solve numerically. New numerical techniques are needed to develop an effective nuSMPBIC finite element solver.

3 A submodel partition of the nuSMPBIC model

One major difficulty in the numerical solution of the nuSMPBIC model comes from the solution singularity caused by the Dirac-delta distributions $\delta_{\mathbf{r}_j}$. Following what are done

in [18, 20], in this section, we partition the nuSMPBIC model into three submodels, called Models 1, 2, and 3, to overcome the singularity difficulty.

Model 1 is defined by the Poisson equation over the whole space $\mathbb{R}^3$,

$$-\epsilon_p \Delta G(\mathbf{r}) = \alpha \sum_{j=1}^{n_p} z_j \delta_{\mathbf{r}_j}, \quad \mathbf{r} \in \mathbb{R}^3, \quad G(\mathbf{r}) \to 0 \text{ as } |\mathbf{r}| \to \infty, \tag{10}$$

whose solution G gives an electrostatic potential induced by atomic charges from an ion channel protein. The analytical solution G of Model 1 and its gradient vector $\nabla G(\mathbf{s})$ can be found in the algebraic expressions [18]

$$G(\mathbf{r}) = \frac{\alpha}{4\pi\epsilon_p} \sum_{j=1}^{n_p} \frac{z_j}{|\mathbf{r}-\mathbf{r}_j|}, \qquad \nabla G(\mathbf{r}) = -\frac{\alpha}{4\pi\epsilon_p} \sum_{j=1}^{n_p} z_j \frac{(\mathbf{r}-\mathbf{r}_j)}{|\mathbf{r}-\mathbf{r}_j|^3} \qquad \forall \mathbf{r} \neq \mathbf{r}_j. \tag{11}$$

Model 2 is defined by the linear interface boundary value problem:

$$\begin{cases} \Delta\Psi(\mathbf{r}) = 0, & \mathbf{r} \in D_m \cup D_p \cup D_s, \\ \Psi(\mathbf{s}^-) = \Psi(\mathbf{s}^+), \quad \epsilon_p \frac{\partial \Psi(\mathbf{s}^-)}{\partial \mathbf{n}_p(\mathbf{s})} = \epsilon_s \frac{\partial \Psi(\mathbf{s}^+)}{\partial \mathbf{n}_p(\mathbf{s})} + (\epsilon_s - \epsilon_p) \frac{\partial G(\mathbf{s})}{\partial \mathbf{n}_p(\mathbf{s})}, & \mathbf{s} \in \Gamma_p, \\ \Psi(\mathbf{s}^-) = \Psi(\mathbf{s}^+), \quad \epsilon_m \frac{\partial \Psi(\mathbf{s}^-)}{\partial \mathbf{n}_m(\mathbf{s})} = \epsilon_s \frac{\partial \Psi(\mathbf{s}^+)}{\partial \mathbf{n}_m(\mathbf{s})} + (\epsilon_s - \epsilon_m) \frac{\partial G(\mathbf{s})}{\partial \mathbf{n}_m(\mathbf{s})} + \tau\sigma, & \mathbf{s} \in \Gamma_m, \\ \Psi(\mathbf{s}^-) = \Psi(\mathbf{s}^+), \quad \epsilon_p \frac{\partial \Psi(\mathbf{s}^-)}{\partial \mathbf{n}_p(\mathbf{s})} = \epsilon_m \frac{\partial \Psi(\mathbf{s}^+)}{\partial \mathbf{n}_p(\mathbf{s})} + (\epsilon_m - \epsilon_p) \frac{\partial G(\mathbf{s})}{\partial \mathbf{n}_p(\mathbf{s})}, & \mathbf{s} \in \Gamma_{pm}, \\ \Psi(\mathbf{s}) = g(\mathbf{s}) - G(\mathbf{s}), & \mathbf{s} \in \Gamma_D, \\ \frac{\partial \Psi(\mathbf{s})}{\partial \mathbf{n}_b(\mathbf{s})} = -\frac{\partial G(\mathbf{s})}{\partial \mathbf{n}_b(\mathbf{s})}, & \mathbf{s} \in \Gamma_N, \end{cases} \tag{12}$$

Clearly, both Models 1 and 2 are independent of ionic concentration c_i. Hence, they can be solved prior to a search for ionic concentrations c_i.

With Models 1 and 2, we can simplify the nuSMPBIC model (8) into Model 3 — a nonlinear system of an electrostatic potential, $\tilde{\Phi}$, (induced purely by ionic charges) and ionic concentration functions c_i as follows:

$$\begin{cases} c_i(\mathbf{r}) - c_i^b \left[1 - \gamma \sum_{j=1}^{n} v_j c_j(\mathbf{r})\right]^{\frac{v_i}{v_0}} e^{-Z_i[G(\mathbf{r})+\Psi(\mathbf{r})+\tilde{\Phi}(\mathbf{r})]} = 0, & \mathbf{r} \in D_s,\ i = 1, 2, \ldots, n, \\ \Delta\tilde{\Phi}(\mathbf{r}) = 0, & \mathbf{r} \in D_m \cup D_p, \\ \epsilon_s \Delta\tilde{\Phi}(\mathbf{r}) + \beta \sum_{i=1}^{n} Z_i c_i(\mathbf{r}) = 0, & \mathbf{r} \in D_s, \\ \tilde{\Phi}(\mathbf{s}^+) = \tilde{\Phi}(\mathbf{s}^-), \quad \epsilon_s \frac{\partial \tilde{\Phi}(\mathbf{s}^+)}{\partial \mathbf{n}_p(\mathbf{s})} = \epsilon_p \frac{\partial \tilde{\Phi}(\mathbf{s}^-)}{\partial \mathbf{n}_p(\mathbf{s})}, & \mathbf{s} \in \Gamma_p, \\ \tilde{\Phi}(\mathbf{s}^+) = \tilde{\Phi}(\mathbf{s}^-), \quad \epsilon_s \frac{\partial \tilde{\Phi}(\mathbf{s}^+)}{\partial \mathbf{n}_m(\mathbf{s})} = \epsilon_m \frac{\partial \tilde{\Phi}(\mathbf{s}^-)}{\partial \mathbf{n}_m(\mathbf{s})}, & \mathbf{s} \in \Gamma_m, \\ \tilde{\Phi}(\mathbf{s}^-) = \tilde{\Phi}(\mathbf{s}^+), \quad \epsilon_p \frac{\partial \tilde{\Phi}(\mathbf{s}^-)}{\partial \mathbf{n}_p(\mathbf{s})} = \epsilon_m \frac{\partial \tilde{\Phi}(\mathbf{s}^+)}{\partial \mathbf{n}_p(\mathbf{s})}, & \mathbf{s} \in \Gamma_{pm}, \\ \tilde{\Phi}(\mathbf{s}) = 0, & \mathbf{s} \in \Gamma_D, \\ \frac{\partial \tilde{\Phi}(\mathbf{s})}{\partial \mathbf{n}_b(s)} = 0, & s \in \Gamma_N. \end{cases} \tag{13}$$

After solving Models 2 and 3, we construct the electrostatic potential function u by the formula

$$u(\mathbf{r}) = G(\mathbf{r}) + \Psi(\mathbf{r}) + \tilde{\Phi}(\mathbf{r}) \qquad \forall \mathbf{r} \in \Omega. \tag{14}$$

Since G collects all the singularity points of u, both Models 2 and 3 can be much easier to solve numerically than the original nuSMPBIC model. Consequently, the complexity of solving the nuSMPBIC model is sharply reduced. An efficient finite element method for solving Model 2 has been reported in [20, 21]. Hence, we only need to develop a finite element method for solving Model 3 as done in the next section.

4 A damped two-block iterative method for solving Model 3

We start with a construction of two finite element meshes — an interface fitted irregular tetrahedral mesh, Ω_h, of a box domain Ω and a tetrahedral mesh, $D_{s,h}$, of a solvent domain D_s. We then use them construct two linear Lagrange finite element function spaces, denoted by $\mathcal{U}$ and $\mathcal{V}$, as two finite dimensional subspaces of the Sobolev function spaces $H^1(\Omega)$ and $H^1(D_s)$ [1], respectively. We further construct a restriction operator, $\mathcal{R} : \mathcal{U} \to \mathcal{V}$, and a prolongation operator, $\mathcal{P} : \mathcal{V} \to \mathcal{U}$, such that $\mathcal{R}u \in \mathcal{V}$ for any $u \in \mathcal{U}$ and $\mathcal{P}c_i \in \mathcal{U}$ for any $c_i \in \mathcal{V}$. With these spaces and operators, we can obtain a finite element approximation of Model 3 as follows: Find $\tilde{\Phi} \in \mathcal{U}_0$ and $c_i \in \mathcal{V}$ for $i = 1, 2, \ldots, n$ such that

$$c_i(\mathbf{r}) - c_i^b \left[1 - \gamma \sum_{j=1}^{n} v_j c_j(\mathbf{r})\right]^{\frac{v_i}{v_0}} e^{-Z_i \mathcal{R}[G(\mathbf{r}) + \Psi(\mathbf{r}) + \tilde{\Phi}(\mathbf{r})]} = 0, \quad \mathbf{r} \in D_{s,h}, \quad i = 1, 2, \ldots, n, \tag{15a}$$

$$a(\tilde{\Phi}, v) - \beta \sum_{j=1}^{n} Z_j \int_{D_s} \mathcal{P}c_j(\mathbf{r}) v d\mathbf{r} = 0 \qquad \forall v \in \mathcal{U}_0, \tag{15b}$$

where $\mathcal{U}_0 = \{u \in \mathcal{U} \mid u = 0 \text{ on } \Gamma_D\}$, which is a subspace of $\mathcal{U}$, and $a(\cdot, \cdot)$ is a bilinear form defined by

$$a(u, v) = \epsilon_p \int_{D_p} \nabla u \cdot \nabla v d\mathbf{r} + \epsilon_m \int_{D_m} \nabla u \cdot \nabla v d\mathbf{r} + \epsilon_s \int_{D_s} \nabla u \cdot \nabla v d\mathbf{r}, \quad u, v \in \mathcal{U}. \tag{16}$$

We now present the damped two-block iterative method for solving the finite element system (15). Here we divide the unknown functions of (15) into two blocks with Block 1 containing all the ionic concentration functions c_i and Block 2 containing $\tilde{\Phi}$ only. With vector $c = (c_1, c_2, \ldots, c_n)$, we rewrite (15a) in the vector equation

$$F(c(\mathbf{r}), \tilde{\Phi}(\mathbf{r})) = \mathbf{0} \quad \forall \mathbf{r} \in D_{s,h}, \tag{17}$$

where $F = (f_1, f_2, \ldots, f_n)$ with the i-th component function f_i being defined by

$$f_i(c(\mathbf{r}), \tilde{\Phi}(\mathbf{r})) = c_i(\mathbf{r}) - c_i^b \left[1 - \gamma \sum_{j=1}^{n} v_j c_j(\mathbf{r})\right]^{\frac{v_i}{v_0}} e^{-Z_i \mathcal{R}[G(\mathbf{r}) + \Psi(\mathbf{r}) + \tilde{\Phi}(\mathbf{r})]}, \quad \mathbf{r} \in D_{s,h}, \quad i = 1, 2, \ldots, n. \tag{18}$$

Thus, (15) has been rewritten in a two block form — a system of (17) and (15b).

Let $(c^k, \tilde{\Phi}^k)$ denote the k-th iterate of the damped two-block iterative method with $c^k = (c_1^k, c_2^k, \ldots, c_n^k)$. When an initial iterate, $(c^0, \tilde{\Phi}^0)$, is given, we define the damped two-block iterative method as follows:

$$c^{k+1}(\mathbf{r}) = c^k(\mathbf{r}) + \omega \left[p(\mathbf{r}) - c^k(\mathbf{r})\right], \quad \mathbf{r} \in D_{s,h}, \tag{19a}$$

$$\tilde{\Phi}^{k+1}(\mathbf{r}) = \tilde{\Phi}^k(\mathbf{r}) + \omega \left[q(\mathbf{r}) - \tilde{\Phi}^k(\mathbf{r})\right], \quad \mathbf{r} \in \Omega, \quad k = 0, 1, 2, \ldots, \tag{19b}$$

where ω is a damping parameter between 0 and 1, $p = (p_1, p_2, \ldots, p_n)$ is a solution of the nonlinear algebraic system

$$F(p(\mathbf{r}), \tilde{\Phi}^k(\mathbf{r})) = \mathbf{0}, \quad \mathbf{r} \in D_{s,h}, \tag{20}$$

and q is a solution of the linear finite element variational problem: Find $q \in \mathcal{U}_0$ such that

$$a(q, v) = \beta \sum_{j=1}^{n} Z_j \int_{D_s} \mathcal{P} c_j^{k+1}(\mathbf{r}) v d\mathbf{r} \quad \forall v \in \mathcal{U}_0. \tag{21}$$

In the implementation, we use the following iteration termination rules:

$$\|\tilde{\Phi}^{k+1} - \tilde{\Phi}^k\|_\Omega < \epsilon, \quad \max_{1 \le i \le n} \|c_i^{k+1} - c_i^k\|_{D_s} < \epsilon, \quad \text{and} \quad R(c^{k+1}, \tilde{\Phi}^{k+1}) < \epsilon, \tag{22}$$

where ϵ is a tolerance (by default, $\epsilon = 10^{-4}$), $\|\cdot\|_\Omega$ and $\|\cdot\|_{D_s}$ denote the norms of function spaces $L_2(\Omega)$ and $L_2(D_s)$, respectively, and $R(c, \tilde{\Phi})$ denotes a residual error of the nonlinear algebraic system (17) as below:

$$R(c, \tilde{\Phi}) = \frac{1}{N_h} \max_{1 \le i \le n} \left(\sum_{\mu=1}^{N_h} \left| f_i(c(\mathbf{r}^{(\mu)}), \tilde{\Phi}(\mathbf{r}^{(\mu)}) \right|^2 \right)^{1/2}. \tag{23}$$

Here $\mathbf{r}^{(\mu)}$ denotes the μ-th mesh point of $D_{s,h}$ and N_h is the total number of mesh points. Clearly, $R(c, \tilde{\Phi}) = 0$ if and only if $F(c(\mathbf{r}), \tilde{\Phi}(\mathbf{r})) = \mathbf{0}$ for $\mathbf{r} \in D_s$. We stop the iterative process (19) and output the $(k+1)$-th iterate $(c^{k+1}, \tilde{\Phi}^{k+1})$ as an approximate solution $(c, \tilde{\Phi})$ of Model 3 whenever the iteration termination rules (22) are satisfied.

5 A Newton iterative method for solving a nonlinear algebraic system of Block 1

In this section, we present a novel Newton iterative scheme for solving the nonlinear algebraic system (20) of Block 1. It is this efficient scheme that turns the damped two-block iterative method (19) into an efficient algorithm for solving Model 3.

A construction of such a Newton iterative scheme is motivated from one basic property of a linear finite element function. That is, a linear finite element function is determined uniquely by its mesh node values. In other words, to search for a unknown linear finite

element function, we only need to determine its mesh node values. According to this property, we set $\mathbf{r} = \mathbf{r}^{(\mu)}$ in the equation of (20) to produce N_h small nonlinear systems as follows:

$$\bar{F}(\xi_\mu) = \mathbf{0}, \quad \mu = 1, 2, \ldots, N_h, \tag{24}$$

where $\xi_\mu = (\xi_{1,\mu}, \xi_{2,\mu}, \ldots, \xi_{n,\mu})$ with $\xi_{i,\mu}$ denoting the mesh node value $p_i(\mathbf{r}^{(\mu)})$ of p_i and $\bar{F} = \left(\bar{f}_1, \bar{f}_2, \ldots, \bar{f}_n\right)$ with $\bar{f}_i$ being defined by

$$\bar{f}_i(\xi_\mu) = \xi_{i,\mu} - c_i^b \left[1 - \gamma \sum_{j=1}^{n} v_j \xi_{j,\mu}\right]^{\frac{v_i}{v_0}} e^{-Z_i u_{k,\mu}} \qquad \text{with} \qquad u_{k,\mu} = G(\mathbf{r}^{(\mu)}) + \Psi(\mathbf{r}^{(\mu)}) + \tilde{\Phi}^k(\mathbf{r}^{(\mu)}).$$

Here $u_{k,\mu}$ is a known value but may be too large to cause a numerical overflow problem during an iterative process. To avoid the overflow problem, for a given allowable upper bound M, we modify $u_{k,\mu}$ as $-M/Z_i$ whenever $-Z_i u_{k,\mu} \geq M$. By default, we set $M = 45$.

Clearly, the N_h nonlinear systems of (24) are independent each other. Hence, they can be solved one-by-one independently to produce nN_h mesh node values $p_i(\mathbf{r}^{(\mu)})$ for $i = 1, 2, \ldots, n$ and $\mu = 1, 2, \ldots, N_h$. We then use them to derive a solution of the nonlinear algebraic system (20).

We now construct a Newton iterative scheme for solving each small nonlinear system of (24). Let ξ_μ^j denote the j-th iterate of the Newton iterative scheme. When an initial iterate ξ_μ^0 is given (by default, $\xi_\mu^0 = c^k$), we define the Newton iterative scheme by

$$\xi_\mu^{j+1} = \xi_\mu^j + \Upsilon_j, \quad j = 0, 1, 2, \ldots, \tag{25}$$

where Υ_j is a solution of the Newton equation

$$J(\xi_\mu^j)\Upsilon_j = -\bar{F}(\xi_\mu^j). \tag{26}$$

Here J denotes a $n \times n$ Jacobian matrix of $\bar{F}$ with the (i, j)-th entry being the partial derivatives $\partial \bar{f}_i / \partial \xi_{j,\mu}$ for $i, j = 1, 2, \ldots, n$ as follows:

$$\frac{\partial \bar{f}_i}{\partial \xi_{j,\mu}} = \begin{cases} 1 + \gamma \frac{v_i^2}{v_0} c_i^b e^{-Z_i u_{k,\mu}} \left[1 - \gamma \sum_{j=1}^{n} v_j \xi_{j,\mu}\right]^{\frac{v_i}{v_0} - 1}, & j = i, \\ \gamma \frac{v_i v_j}{v_0} c_i^b e^{-Z_i u_{k,\mu}} \left[1 - \gamma \sum_{j=1}^{n} v_j \xi_{j,\mu}\right]^{\frac{v_i}{v_0} - 1}, & j \neq i. \end{cases} \tag{27}$$

Each Newton equation (26) can be solved directly by the Gaussian elimination method since n is small (say 2, 3, or 4). When $\|\Upsilon_j\| < \epsilon$ (by default $\epsilon = 10^{-8}$), we output ξ_μ^{j+1} as a numerical solution of (24).

6 A good initial iterate for the damped two-block iterative method

When all the ion sizes v_i are set to be equal to the average size $\bar{v} = \frac{1}{n}\sum_{i=1}^{n} v_i$, we can solve the nonlinear algebraic system (7) for c to derive an analytical expression of c_i as follows:

$$c_i(\mathbf{r}) = \frac{c_i^b e^{-Z_i u(\mathbf{r})}}{1 + \gamma \frac{\bar{v}^2}{v_0} \sum_{j=1}^{n} c_j^b e^{-Z_j u(\mathbf{r})}}, \quad \mathbf{r} \in D_s, \quad i = 1, 2, \ldots, n. \tag{28}$$

Substituting the above expressions to the finite element equation (15b) and using the formula $u = G + \Psi + \tilde{\Phi}$, we can obtain the following nonlinear finite element variational problem: Find $\tilde{\Phi} \in \mathcal{U}_0$ such that

$$a(\tilde{\Phi}, v) - \beta \int_{D_s} \frac{\sum_{i=1}^{n} Z_i c_i^b e^{-Z_i(G+\Psi+\tilde{\Phi})}}{1 + \gamma \frac{\bar{v}^2}{v_0} \sum_{i=1}^{n} c_i^b e^{-Z_i(G+\Psi+\tilde{\Phi})}} v d\mathbf{r} = 0 \quad \forall v \in \mathcal{U}_0, \tag{29}$$

Using the Taylor expansion $e^x = 1 + x + O(x^2)$ and the electroneutrality condition $\sum_{i=1}^{n} Z_i c_i^b = 0$, we can linearize the nonlinear problem (29) as the following linear finite element equation: Find $\tilde{\Phi} \in \mathcal{U}_0$ such that

$$a(\tilde{\Phi}, v) + \bar{\beta} \int_{D_s} \tilde{\Phi} v d\mathbf{r} = -\bar{\beta} \int_{D_s} (G + \Psi) v d\mathbf{r} \quad \forall v \in \mathcal{U}_0. \tag{30}$$

where $\bar{\beta}$ is defined by

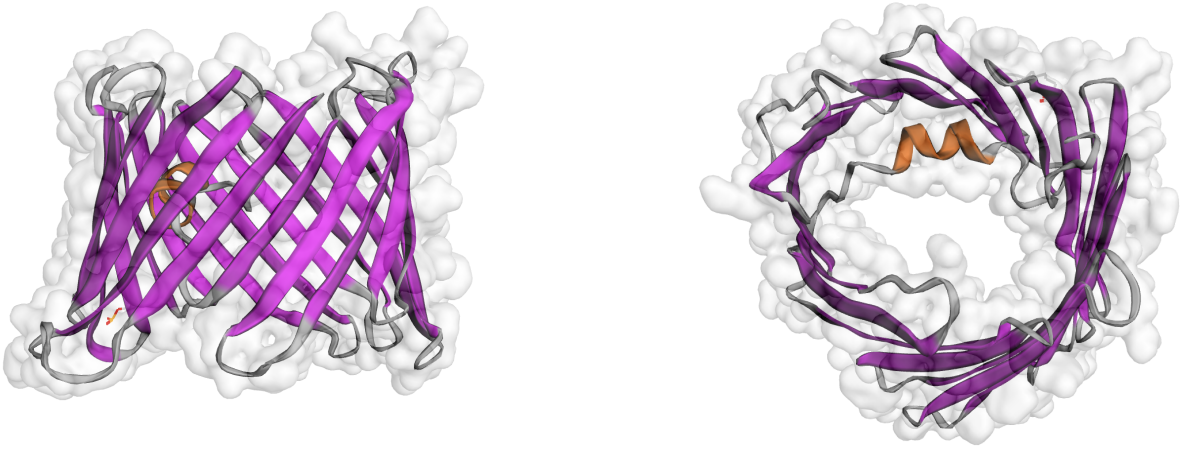
$$\bar{\beta} = \frac{\beta \sum_{i=1}^{n} Z_i^2 c_i^b}{1 + \gamma \frac{\bar{v}^2}{v_0} \sum_{i=1}^{n} c_i^b}.$$

A solution of the above linear equation is selected as an initial iterate $\tilde{\Phi}^{(0)}$ of the damped two-block iterative method (19). We then use the formula (28) to get the initial iterates c_i^0 by

$$c_i^0(\mathbf{r}) = \frac{c_i^b e^{-Z_i[G(\mathbf{r})+\Psi(\mathbf{r})+\tilde{\Phi}^0(\mathbf{r})]}}{1 + \gamma \frac{\bar{v}^2}{v_0} \sum_{j=1}^{n} c_j^b e^{-Z_j[G(\mathbf{r})+\Psi(\mathbf{r})+\tilde{\Phi}^0(\mathbf{r})]}}, \quad \mathbf{r} \in D_s, \quad i = 1, 2, \ldots, n. \tag{31}$$

7 Program package and numerical results

We have presented a nuSMPBIC finite element solver in the above sections. For clarity, we summarize it in Algorithm 1. We then implemented it in Python and Fortran as a software package based on the state-of-the-art finite element library from the FEniCS project [13] and the Poisson-Boltzmann finite element program packages reported in [18, 19, 20]. Here the linear interface boundary value problem (12) of Model 2 is solved by the efficient



(a) Side view of mVDAC1 (b) Top view of mVDAC1

Figure 2: A crystallographic three-dimensional molecular structure of mVDAC1 (PDB ID: 3EMN) depicted in cartoon representations. Here the Van der Waals volume (a volume occupied by all the individual atomic balls of mVDAC1) is also displayed in grey color.

finite element method reported in [20, 21] while other related linear finite element equations are solved approximately by a generalized minimal residual method using incomplete LU preconditioning (GMRES-ILU) with the absolute and relative residual error tolerances being 10^{-6} by default.

Algorithm 1 (The nuSMPBIC finite element solver). *Let $\mathcal{U}$ and $\mathcal{V}$ be linear Lagrange finite element spaces of $H^1(\Omega)$ and $H^1(Ds)$, respectively, and $(c^k, \tilde{\Phi}^k)$ with $c^k = (c_1^k, c_2^k, \ldots, c_n^k)$ be the k-th iterate of the damped two-block iterative method (19). A finite element solution (u, c) of the nuSMPBIC model (8) with $c = (c_1, c_2, \ldots, c_n)$ is calculated in the following four steps:*

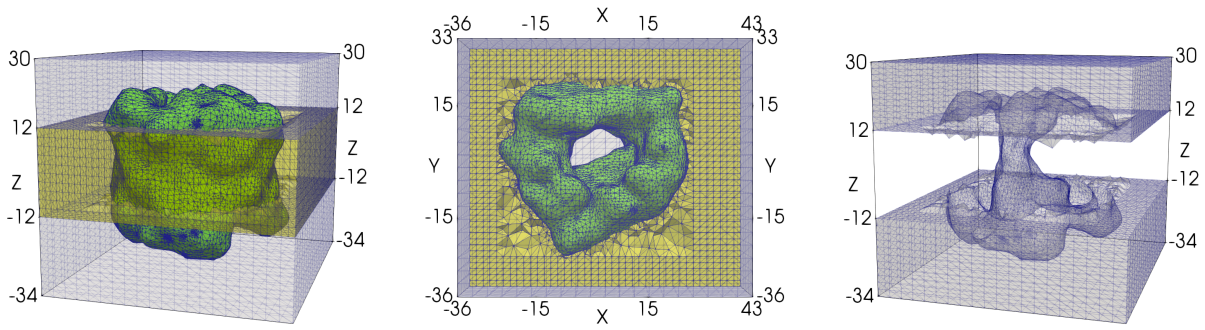
Step 1. Initialization:

- *(a) Calculate G and ∇G via (11) on $\mathcal{U}$.*
- *(b) Solve Model 2 for Ψ on $\mathcal{U}$.*
- *(c) Calculate $\tilde{\Phi}^0$ by solving the linear finite element equation (30) on $\mathcal{U}$ and c^0 by formula (31).*
- *(d) Set $k = 0$.*

Step 2. Calculate $(c^{k+1}, \tilde{\Phi}^{k+1})$ by the damped two-block iterative method (19). Here the nonlinear algebraic system (20) is solved by the Newton iterative scheme (25).

Step 3. Check the convergence: If (22) holds, set $(c^{k+1}, \tilde{\Phi}^{k+1})$ as an approximate solution of Model 3 and go to Step 4; otherwise, increase k by 1 and go back to Step 2.

Step 4. Construct u by the solution decomposition (14): $u(\mathbf{r}) = G(\mathbf{r}) + \Psi(\mathbf{r}) + \tilde{\Phi}(\mathbf{r}) \quad \forall \mathbf{r} \in \Omega$.



(a) Box domain mesh Ω_h (b) Top view of Ω_h (c) Solvent region mesh $D_{s,h}$

Figure 3: (a, b) Two views of an interface fitted irregular tetrahedral mesh Ω_h of a box domain Ω. (c) An irregular tetrahedral mesh $D_{s,h}$ of the solvent region D_s extracted from Ω_h. Here the meshes of the membrane region D_m and protein region D_p are colored in yellow and green and the two solvent compartments above and below the membrane belong to the cytoplasm and intermembrane space, respectively.

To demonstrate the convergence of the damped two-block iterative method for solving Model 3 and the performance of our nuSMPBIC finite element package, we did numerical tests on a murine voltage-dependent anion channel 1 (mVDAC1) [17] in a mixture of 0.1 mole KNO_3 (potassium nitrate) and 0.1 mole NaCl (table salt). Here the four ionic species Cl^-, NO_3^-, K^+, and Na^+ were ordered from 1 to 4 for their concentration functions c_i, bulk concentrations $c_i^b = 0.1$, and charge numbers $Z_1 = -1, Z_2 = -1, Z_3 = 1$, and $Z_4 = 1$. We treated each ion as a ball to estimate v_i via the ball volume formula $v_i = 4\pi r_i^3/3$ with r_i denoting an ionic radius in Å. From the website *https://bionumbers.hms.harvard.edu/bionumber.aspx?&id=108517* we got

$$r_1 = 1.81,\ r_2 = 2.64,\ r_3 = 1.33,\ r_4 = 0.95.$$

Using them, we obtained the four ion sizes v_i and their average volume $\hat{v} = (v_1+v_2+v_3+v_4)/4$ as follows:

$$v_1 = 24.8384, \quad v_2 = 77.0727, \quad v_3 = 9.8547, \quad v_4 = 3.5914, \quad \hat{v} = 28.8393.$$

This mixture is a good selection for us to demonstrate the importance of considering distinct ion sizes since it contains two anions with the same charge number -1 (Cl^- and NO_3^-) and two cations with the same charge number $+1$ (K^+ and Na^+) and have four significantly different ion sizes.

As the main conduit on the outer mitochondrial membrane for the entry and exit of ions and metabolites between the cytosol and the mitochondria, the mVDAC1 has various ionic species with very different ion sizes within its channel pore, making it a good test case for us to validate the nuSMPBEic model not mention its anion-selectivity property and complex molecular structure [17]. We used a crystallographic three-dimensional molecular structure of mVDAC1 from the Orientations of Proteins in Membranes (OPM) database (*https://opm.phar.umich.edu*), instead of the Protein Data Bank (PDB) (*https://www.rcsb.org*), since in the OPM database, the mVDAC1 structure has been manipulated exactly like what

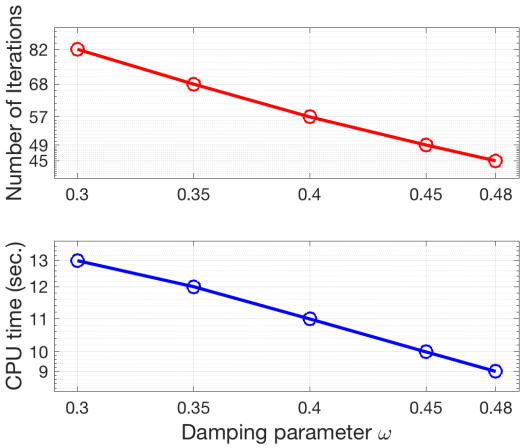


Figure 4: Convergence and performance of the damped two-block iterative method (19) for a finite element system (15) of Model 3 as functions of ω for a mVDAC1 (PDB ID: 3EMN) in a mixture solution with four ionic species Cl^-, Na^+, K^+, and NO_3^-.

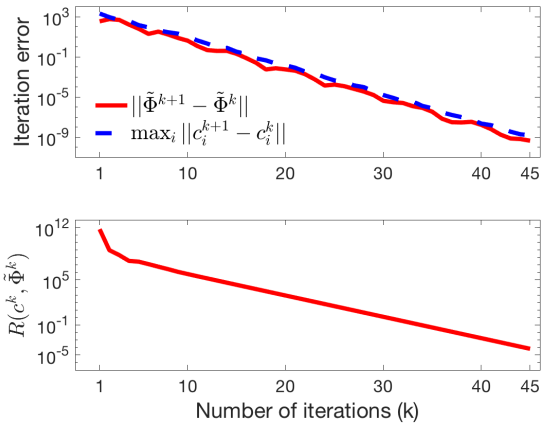


Figure 5: Iteration errors and residual errors of the damped two-block iterative method using $\omega = 0.48$ for solving a nonlinear finite element system (15) of Model 3 as functions of the number k of iterations. Here the residual error $R(c, \tilde{\Phi})$ is defined in (23).

we need as illustrated in Figure 1, together with the membrane location numbers $Z1 = -12$ Å and $Z2 = 12$ Å. This ion channel protein has 4313 atoms and 283 amino acids in one α-helix and one β-barrel (with 19 β-strands) as depicted in Figure 2. The β-barrel has height 35 Å and width 40 Å. The channel pore has the width 27 Å at the entrance and 14 Å at the center. After downloading a PDB file from the OPM database (with the PDB identification (ID): 3EMN), we converted it to a PQR file on the PDB2PQR web server (*http://nbcr-222.ucsd.edu/pdb2pqr_2.1.1/*) to get the data missed in the PDB file such as hydrogen atoms, the atomic charge numbers, and atomic radii. Such a PQR file is a required input data file for our program package.

We constructed a box domain Ω using $L_{x1} = -36, L_{x2} = 43, L_{y1} = -36, L_{y2} = 33, L_{z1} = -34$, and $L_{z2} = 30$ and generated an interface fitted irregular tetrahedral mesh Ω_h of Ω (with 49798 mesh points) by an ion channel finite element mesh program package [4, 12]. We then extracted a solvent region mesh $D_{s,h}$ from the box domain mesh Ω_h (with 29366 mesh points). From Figure 3 it can be seen that these two meshes Ω_h and $D_{s,h}$ are very irregular due to the complex interfaces Γ_p and Γ_{pm} or a complex molecular surface of mVDAC1.

All the numerical tests were done on an iMac computer with one 4.2 GHz Intel core i7 processor and 64 GB memory. For simplicity, we fixed the parameters $\epsilon_p = 2$, $\epsilon_m = 2$, $\epsilon_s = 80$, $u_b = 0$, and $u_t = 0$ in these tests. The numerical test results are reported in Table 1 and Figures 4 to 9.

Figure 4 reports the convergence and performance of our damped two-block iterative method (19) in terms of the number of iterations and computer CPU time. From the figure it can be seen that the number of iterations and CPU time were reduced monotonically for $\omega \leq 0.48$. The damped two-block iterative method was found to be divergent for $\omega > 0.48$. At $\omega = 0.48$, it took about 12.63 seconds only to find one electrostatic potential and four ionic concentrations as a finite element solution of Model 3. These tests demonstrate the

fast convergence of our damped two-block iterative method and the high performance our nuSMPBIC finite element package.

Figure 5 displays a convergence process of the damped two-block iterative method using $\omega = 0.48$ in terms two iteration errors $\|\tilde{\Phi}^{k+1} - \tilde{\Phi}^k\|_\Omega$ and $\max_{1\le i\le n} \|c_i^{k+1} - c_i^k\|_{D_s}$ and one residual error $R(c^k, \tilde{\Phi}^k)$ defined in (23). From the figure it can be seen that this iterative method quickly reduced the two iteration errors from about 10^3 to 10^{-9} in 45 iterations and the residual error from 10^{12} to 10^{-5}, which indicates that the finite element solution of Model 3 has well reflected the ion size effects since it satisfied the size constraint conditions (7) in high accuracy.

Table 1: A comparison of the performance of our nuSMPBIC finite element solver using the GMRES-ILU iterative method with that using the Gaussian elimination direct method in terms of computer CPU times in seconds. Here $\omega = 0.48$.

Linear solver	Calculate G & ∇G	Solve Model 2 for Ψ	Solve (30) for $\tilde{\Phi}^0$	Solve Model 3 for $(c, \tilde{\Phi})$	Total CPU time
GMRES-ILU	1.13	0.91	0.60	9.37	12.01
Direct	1.19	2.74	2.55	12.63	19.11

Table 1 lists the distribution of computer CPU time in the major parts of the nuSMPBIC finite element solver, along with the case using the Gaussian elimination direct method to solve each related linear finite element equation. It shows that the nuSMPBIC finite element solver using the GMRES-ILU iterative method took much less CPU time than that using the Gaussian elimination direct method, demonstrating the efficiency of the GMRES-ILU method in our nuSMPBIC finite element package.

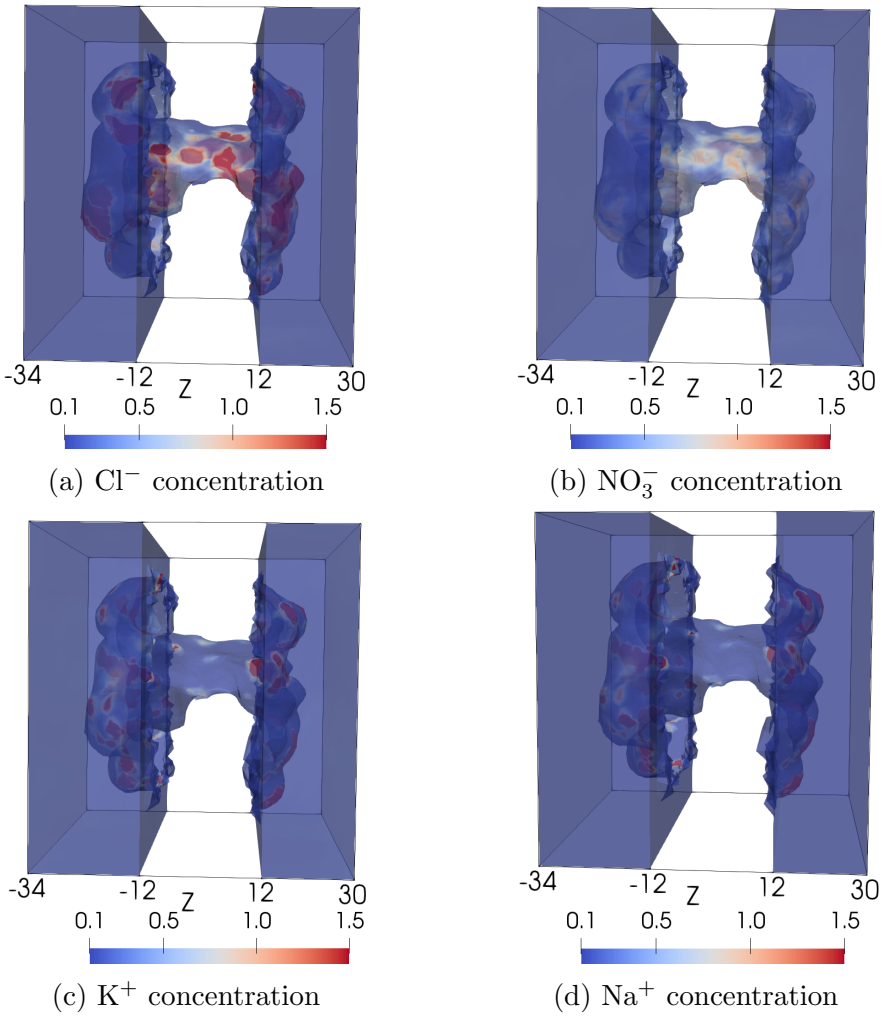
Figure 6 displays the concentrations of ions Cl^-, NO_3^-, K^+, and Na^+ on a surface of the solvent region D_s in color mapping. Here all the concentration values more than 1.5 mol/L and less than 0.1 mole/L have been colored in red and blue, respectively. From Plots (a, b) it can be seen that there are much more anions Cl^- than NO_3^- within the channel pore due to that the ion size of Cl^- is much smaller that that of NO_3^- (i.e., 24.84 vs. 77.07 in $Å^3$) even though both Cl^- and NO_3^- have the same charge number -1 and bulk concentration 0.1 mol/L. In the cation case, Plots (c, d) show that there are few cations K^+ and Na^+ within the channel pore but it is difficult for us to tell which one more or less since each of them only displays one view of a three-dimensional concentration.

Using a curve visualization scheme reported in [21], we calculated the average values c_i^j and $u_j^\pm$ of concentration function c_i and positive/negative part $u^\pm$ of electrostatic potential function u by the formulas

$$c_i^j = \frac{1}{\|B_{j,h}\|}\int_{B_{j,h}} c_i(\mathbf{r})d\mathbf{r}, \quad u_j^\pm = \frac{1}{\|B_{j,h}\|}\int_{B_{j,h}} u^\pm(\mathbf{r})d\mathbf{r}, \quad j = 1, 2, \ldots, m, \tag{32}$$

where $m = 80$, $B_{j,h}$ denotes the jth block mesh of a solvent region mesh $D_{s,h}$, $u^\pm = \frac{1}{2}[u(\mathbf{r}) \pm |u(\mathbf{r})|]$, and $\|B_{j,h}\|$ denotes the volume of block $B_{j,h}$. In particular, $B_{j,h}$ was extracted from $D_{s,h}$ by

$$B_{j,h} = \big([L_{x1}, L_{x2}] \times [L_{y1}, L_{y2}] \times [z^j - \bar{h}/2, z^j + \bar{h}/2]\big) \cap D_{s,h},$$



(a) Cl^- concentration (b) NO_3^- concentration

(c) K^+ concentration (d) Na^+ concentration

Figure 6: The color mappings of the four ionic concentrations generated by the nuSMPBIC finite element program package for mVDAC1 (PDB ID: 3EMN) in a mixture solution of 0.1 molar KNO_3 and 0.1 molar NaCl on one surface view of the solvent region D_s in the Z-axis direction.

where z^j denotes the jth partition number of the interval $[L_{z1} + \bar{h}/2, L_{z2} - \bar{h}/2]$ with $\bar{h} = 5$ in the z-axis direction. These partition numbers include the membrane location numbers Z_1 and Z_2. In addition, we set $z^0 = L_{z1}$, $z^{m+1} = L_{z2}$, $c_i^0 = c_i^b$, $c_i^{m+1} = c_i^b$, $u_0^{\pm} = u_b$, and $u_{m+1}^{\pm} = u_t$. Using these points (z^j, c_i^j) and $(z^j, u_j^{\pm})$ for $j = 0, 1, 2, \ldots, m, m+1$, we plotted 2D curves and displayed them in Figure 7. Here the central part of the channel pore that links to membrane (i.e., $-12 \leq z \leq 12$) has been highlighted in light-cyan while the other parts of the channel pore in green to let us more clearly view the distribution profiles of c_i and $u^{\pm}$ within the central part of the channel pore.

From Figure 7 it can be seen that the positive potential u^+ is much stronger than the negative potential u^-, causing anions Cl^- and NO_3^- to expel most cations K^+ and Na^+ away from the central portion of a channel pore between $Z1 < z < Z2$ highlighted in light-cyan. We also can see that the maximum concentration value of Cl^- is almost triple that of NO_3^-

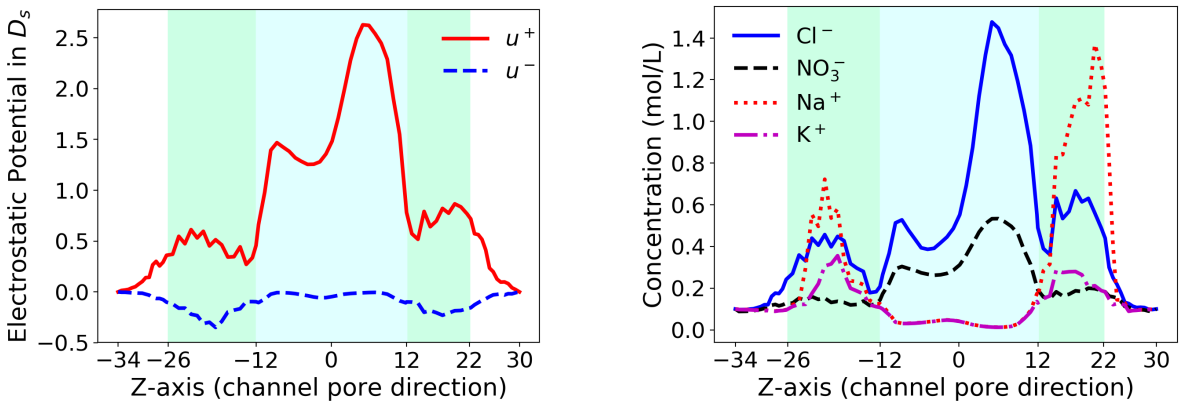


Figure 7: The electrostatic potentials u^+ and u^- and ionic concentrations c_i generated by our nuSMPBIC finite element program package for mVDAC1 (PDB ID: 3EMN) in a mixture solution of 0.1 molar KNO_3 and 0.1 molar NaCl with four ionic species Cl^-, Na^+, K^+, and NO_3^-. Here u^+ and u^- denote the positive and negative parts of electrostatic potential u; the central part of the channel pore that links to the membrane (i.e., $-12 \le z \le 12$) is highlighted in light-cyan; and the other parts of the channel pore are highlighted in green.

(1.48 vs. 0.53) simply because the ion size of Cl^- is much smaller than that of NO_3^- (24.84 vs. 77.07). For cations, we find that the maximum concentration value of Na^+ is almost four times that of K^+ (1.37 vs. 0.36) in the range $12 < z < 22$ highlighted in green since the ion size of K^+ is about triple the ion size of Na^+ (9.85 vs. 3.59). These test results demonstrate that our nuSMPBIC model can well retain the anion selectivity property of mVDAC1 and that ionic sizes have significant impacts on electrostatics and ionic concentrations. They also indicate that the anion selectivity happens mostly within the central part of the ion channel pore.

The new damped two-block iterative method works for a uniform ion size case too. To confirm it, we did numerical tests using $v_i = \hat{v}$ with $\hat{v} = 28.8393$ and $\omega = 0.35$. The test results were reported in Figure 8. In this uniform ion size test case, the damped two-block iterative method took 46 iterations and 11 seconds in computer CPU time to satisfy the iteration convergence rule (22). As shown in Section 6, the nuSMPBIC model can be reduced from a nonlinear system to the nonlinear finite element boundary value problem (29), which defines the SMPBIC model and has been solved by an efficient modified Newton iterative method in [20]. As a comparison, we repeated the test using the SMPBIC finite element package reported in [20]. In this test, the nonlinear finite element equation (29) was solved to satisfy the iteration convergence rule (22) in 8 modified Newton iterations but took about 16 seconds in the total CPU time. This comparison test indicates that the damped two-block iterative method can also be efficient even compared to the modified Newton iterative method for solving the nonlinear finite element equation (29).

However, because all the ions were set to have the same size, the 2D curves of concentrations of the two anion species Cl^- and NO_3^- and the two cation species K^+ and Na^+ are overlapped each other, respectively, in Figure 8, implying that the concentrations of Cl^- and NO_3^- (or K^+ and Na^+) are identical each other. This matches exactly what we could expect in physics when all the ions have the same size, the same charge number (-1 for the anions

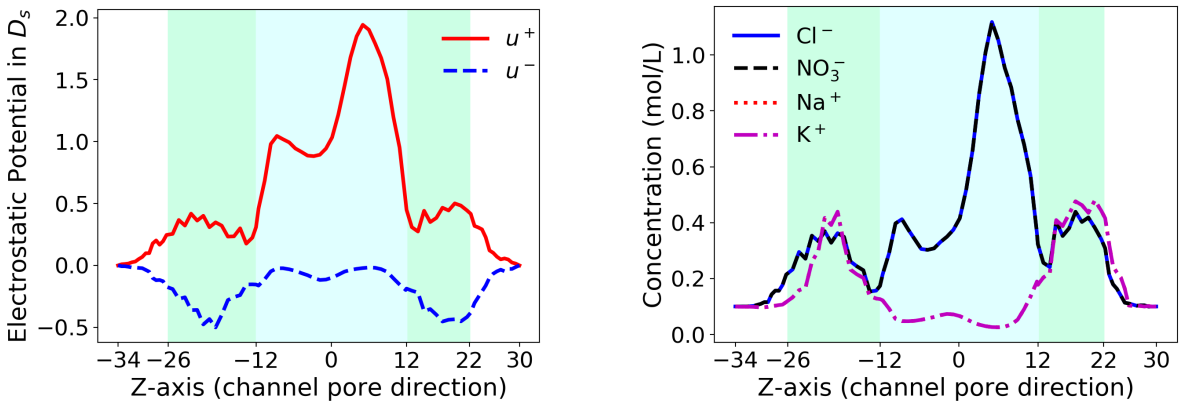


Figure 8: The electrostatic potentials u^+ and u^- and ionic concentrations c_i generated by the nuSMPBIC finite element program package for mVDAC1 (PDB ID: 3EMN) in a mixture solution of 0.1 molar KNO_3 and 0.1 molar NaCl in a uniform ion size case: all the ions are set to have the same average volume size $\hat{v}$. That is, $v_i = \hat{v} = 28.8393$ for $i = 1, 2, 3, 4$ for the four ionic species Cl^-, NO_3^-, K^+, and Na^+.

Cl^- and NO_3^- and $+1$ for the cations K^+ and Na^+), and the same bulk concentration 0.1 mol/L. Even so, these test results still well reflect the anion selectivity property of mVDAC1. Hence, the SMPBIC model can remain a valuable model in ion channel simulation and study due to its simplicity.

Finally, we did tests using the membrane surface charge density $\sigma = 10$ μC/cm^2 to check the affection of membrane charges on a solution of the nuSMPBIC model. The derived potential and concentration functions were reported in Figure 9. From a comparison with those reported in Figure 7 (i.e., the case without considering any membrane charge), we can see that the positive membrane surface charge significantly increased the values of positive electrostatic potential function u^+ and anionic concentrations for Cl^- and NO_3^- but had small affection to the negative electrostatic potential function u^- and cationic concentrations for Na^+ and K^+. This test indicates the importance of considering membrane charges in the calculation of electrostatic potential and ionic concentration functions.

8 Conclusions

We have presented an efficient nuSMPBIC finite element iterative method for solving a nonuniform size modified Poisson-Boltzmann ion channel (nuSMPBIC) model using Neumann-Dirichlet mixed boundary conditions and a membrane surface charge density, along with its finite element program package that works for an ion channel protein with a three-dimensional crystallographic structure, a mixture solution of multiple ionic species, a nonuniform ion size case, and a uniform ion size case. In particular, we divide the nuSMPBIC model into three-submodels, called Models 1, 2, and 3, to overcome the difficulty of solution singularities induced from singular Direct-delta distributions and to sharply reduce the complexity of solving the nuSMPBIC model. We then have developed an efficient damped two-block iterative method for solving a linear finite element approximation to Model 3 — a system

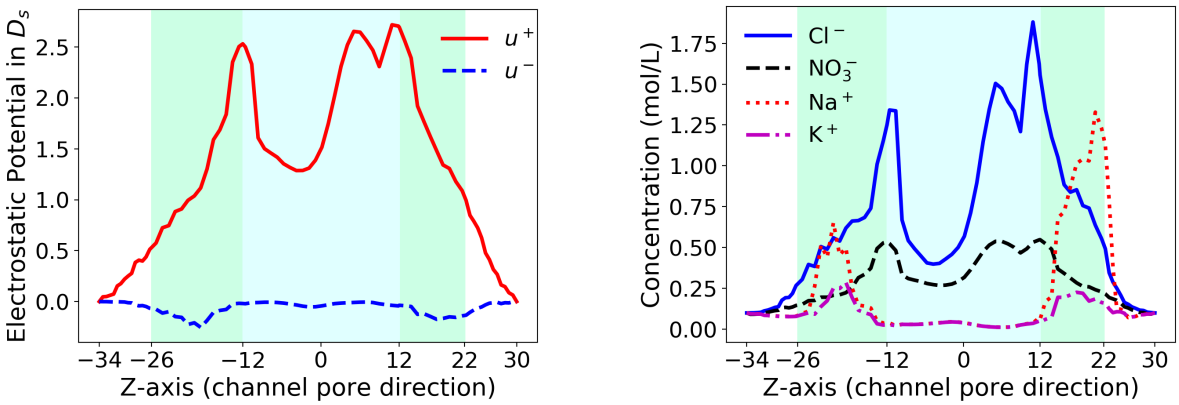


Figure 9: The electrostatic potentials u^+ and u^- and ionic concentrations c_i generated by the nuSMPBIC finite element program package with the membrane surface charge density $\sigma = 10$ μC/cm^2 for mVDAC1 (PDB ID: 3EMN) in a mixture solution of 0.1 molar KNO_3 and 0.1 molar NaCl.

mixing nonlinear algebraic equations with a finite element variational problem, including a novel modified Newton iterative scheme for solving each related nonlinear algebraic system. Numerical test results on a voltage-dependent anion-channel (VDAC) in a mixture of four ionic species have demonstrated the fast convergence of our damped two-block iterative method, the high performance of our finite element package, and the importance of considering nonuniform ion sizes in the calculation of electrostatic potentials and ionic concentrations. The nuSMPBIC model has also well validated by the anion-selectivity property of VDAC.

Since the focus of this paper is on the presentation of the nuSMPBIC model and its finite element solver, we only reported numerical test results for one ion channel protein in this paper. To further confirm the effectiveness and performance of our nuSMPBIC finite element solver, we plan to make numerical experiments on more ion channel proteins and do comparison studies with other ion channel models in our future work. During these new studies, we will further improve the efficiency of the nuSMPBIC finite element iterative method and the quality and usage of the nuSMPBIC finite element package. In this way, our nuSMPBIC finite element package will become a valuable simulation tool not only for quantitative assessment of ion size impacts on ion channel electrostatics and ionic concentrations but also for the study of ion channel selectivity properties, ionic distribution patterns across membrane, and membrane charge effects on electrostatics and ionic concentrations.

Acknowledgements

This work was partially supported by the Simons Foundation, USA, through research award 711776.

References

[1] R. Adams and J. Fournier, *Sobolev Spaces*, Elsevier/Academic Press, Amsterdam, second ed., 2003.

[2] M. Z. Bazant, B. D. Storey, and A. A. Kornyshev, *Double layer in ionic liquids: Overscreening versus crowding*, Phys. Rev. Lett., 106 (2011), p. 046102.

[3] I. Borukhov, D. Andelman, and H. Orland, *Steric effects in electrolytes: A modified Poisson-Boltzmann equation*, Physical Review Letters, 79 (1997), pp. 435–438.

[4] Z. Chao, *Analysis on some basic ion channel modeling problems*, dissertation, The University of Wisconsin-Milwaukee, August 2020.

[5] D. Chen, Z. Chen, C. Chen, W. Geng, and G. Wei, *MIBPB: A software package for electrostatic analysis*, Journal of Computational Chemistry, 32 (2011), pp. 756–770.

[6] B. Honig and A. Nicholls, *Classical electrostatics in biology and chemistry*, Science, 268 (1995), pp. 1144–1149.

[7] E. Jurrus, D. Engel, K. Star, K. Monson, J. Brandi, L. E. Felberg, D. H. Brookes, L. Wilson, J. Chen, K. Liles, et al., *Improvements to the APBS biomolecular solvation software suite*, Protein Science, 27 (2018), pp. 112–128.

[8] B. Li, *Continuum electrostatics for ionic solutions with non-uniform ionic sizes*, Nonlinearity, 22 (2009), pp. 811–833.

[9] J. Li and D. Xie, *An effective minimization protocol for solving a size-modified Poisson-Boltzmann equation for biomolecule in ionic solvent*, International Journal of Numerical Analysis and Modeling, 12 (2015), pp. 286–301.

[10] J. Li, J. Ying, and D. Xie, *On the analysis and application of an ion size-modified Poisson-Boltzmann equation*, Nonlinear Analysis: Real World Applications, 47 (2019), pp. 188–203.

[11] J.-L. Liu and B. Eisenberg, *Poisson-Nernst-Planck-Fermi theory for modeling biological ion channels*, The Journal of chemical physics, 141 (2014), p. 22D532.

[12] T. Liu, S. Bai, B. Tu, M. Chen, and B. Lu, *Membrane-channel protein system mesh construction for finite element simulations*, Computational and Mathematical Biophysics, 3 (2015).

[13] A. Logg, K.-A. Mardal, and G. N. Wells, eds., *Automated Solution of Differential Equations by the Finite Element Method*, vol. 84 of Lecture Notes in Computational Science and Engineering, Springer Verlag, 2012.

[14] R. Luo, L. David, and M. K. Gilson, *Accelerated Poisson–Boltzmann calculations for static and dynamic systems*, Journal of Computational Chemistry, 23 (2002), pp. 1244–1253.

[15] J. M. Ortega and W. C. Rheinboldt, *Iterative Solution of Nonlinear Equations in Several Variables*, Academic Press, 1970.

[16] B. Roux and T. Simonson, *Implicit solvent models*, Biophys. Chem., 78 (1999), pp. 1–20.

[17] R. Ujwal, D. Cascio, J.-P. Colletier, and etc., *The crystal structure of mouse VDAC1 at 2.3 Å resolution reveals mechanistic insights into metabolite gating*, Proceedings of the National Academy of Sciences, 105 (2008), pp. 17742–17747.

[18] D. Xie, *New solution decomposition and minimization schemes for Poisson-Boltzmann equation in calculation of biomolecular electrostatics*, J. Comput. Phys., 275 (2014), pp. 294–309.

[19] D. Xie, *New finite element iterative methods for solving a nonuniform ionic size modified Poisson-Boltzmann equation*, International Journal of Numerical Analysis and Modeling, 14 (2017), pp. 688–711.

[20] D. Xie, S. H. Audi, and R. K. Dash, *A size modified Poisson-Boltzmann ion channel model in a solvent of multiple ionic species: Application to VDAC*, Journal of Computational Chemistry, 41 (2020), pp. 218–231.

[21] D. Xie and Z. Chao, *A finite element iterative solver for a pnp ion channel model with neumann boundary condition and membrane surface charge*, Journal of Computational Physics, 423 (2020. https://doi.org/10.1016/j.jcp.2020.109915).

[22] D. Xie, J.-L. Liu, and B. Eisenberg, *Nonlocal Poisson-Fermi model for ionic solvent*, Physical Review E, 94 (2016), p. 012114.

[23] Y. Xie, J. Ying, and D. Xie, *SMPBS: Web server for computing biomolecular electrostatics using finite element solvers of size modified Poisson-Boltzmann equation*, Journal of Computational Chemistry, 38 (2017), pp. 541–552.

[24] J. Ying and D. Xie, *A hybrid solver of size modified Poisson-Boltzmann equation by domain decomposition, finite element, and finite difference*, Applied Mathematical Modelling, 58 (2018), pp. 166–180.